Supporting information

Intermixing-seeded growth for high-performance planar heterojunction perovskite solar cells assisted by precursor-capped nanoparticles

Shao-Sian Li,[a] Chi-Huang Chang,[b] Ying-Chiao Wang,[a] Chung-Wei Lin,[a] Di-Yan Wang,[c] Jou-Chun Lin,[c] Chia-Chun Chen,[c,d] Hwo-Shuenn Sheu,[e] Hao-Chung Chia,[f] Wei-Ru Wu,[e] U-Ser Jeng*[e,f] Chi-Te Liang,[b] Raman Sankar,[g,h] Fang-Cheng Chou[g,h] and Chun-Wei Chen*[a,h]

[a.] Department of Materials Science and Engineering, National Taiwan University, No.1, Sec. 4, Roosevelt Rd., Taipei, Taiwan. E-mail: chunwei@ntu.edu.tw.

[b.] Department of Physics, National Taiwan University, No.1, Sec. 4, Roosevelt Rd., Taipei, Taiwan.

[c.] Department of Chemistry, National Taiwan Normal University, No. 88, Sec. 4, Ting-Chow Rd, Taipei, Taiwan

[d.] Institute of Atomic and Molecular Sciences, Academia Sinica, No. 1, Sec. 4, Roosevelt Rd, Taipei, Taiwan

[e.] National Synchrotron Radiation Research Center, No. 101, Hsin-An Road, Hsinchu, 30077, Taiwan. E-mail: usjeng@nsrrc.org.tw

[f.] Chemical Engineering Department, National Tsing-Hua University, Hsinchu, 30013, Taiwan

[g.] Center for Condensed Matter Sciences, National Taiwan University, No.1, Sec. 4, Roosevelt Rd., Taipei, Taiwan.

[h.] Taiwan Consortium of Emergent Crystalline Materials (TCECM), Ministry of Science and Technology, No. 1, Sec. 4, Roosevelt Rd, Taipei, Taiwan.

1. Synthesis of PbS nanoparticles and ligand exchange process.

1-1 Synthesis of PbS nanoparticles

The PbS nanocrystals were prepared by the wet solution phase chemical synthesis with some modifications. In brief, 223 mg of PbO and 10 ml of oleic acid were mixed and then were allowed to react under N_2 gas at 150 °C for 60 min to form

the Pb–oleic acid complex. Afterwards, 2.5 ml 1-octadecene solution of bis(trimethylsilylmethyl) sulfide (96 mg) was quickly injected into the solution. The resulting solution was heated to 220 ^{o}C for 60 min. Two washing steps were included to remove un-reacted materials and solvents. After the solution was cooled to room temperature, a large amount of methanol was added to precipitate OA-capped PbS nanoparticles followed by centrifugation. The solid product was dispersed well in octane.

1-2 Ligand exchange process

The as-synthesized PbS nanoparticles capped with OA were first dispersed in octane with various concentrations of 6.5, 13, and 20 mg/ml, whereas halide ligand MAI was dissolved in DMF solvent. To exchange OA ligands in lower concentrations of PbS nanoparticles, such as 6.5 or 13 mg/ml, 8 mg/ml of MAI was sufficient for complete the removal of OA-ligands; however, for a higher concentration of 20 mg/ml PbS nanoparticles, 20 mg/ml of MAI was required. After mixing these two solutions vigorously, it was kept static until octane and DMF well phase-separated and MAI-capped PbS nanoparticles could transfer into the DMF solution.

2. **Preparation of perovskite precursor solution with the addition of PbS nanoparticles.**

A small amount of MAI-capped PbS nanoparticles after ligand exchange treatment were mixed with the pristine perovskite precursor (MAI and $PbCl_2$) for device fabrications in DMF. A volume of 80 μl of each DMF solution of MAI-capped PbS concentrations of 6.5, 13, or 20 mg/ml, was mixed with 320 μl of the DFM solution of pristine perovskite precursor (molar ratio of MAI and $PbCl_2$ is 3:1, at 40 wt% in DMF), for 0.5, 1.0, or 1.5 wt% of MAI-PbS with respective to the total solute weight of the perovskite precursor and PbS nanoparticles.

3. **Perovskite solar cell fabrication procedures**

FTO glasses were cleaned and then spin-coated with the 0.15 M titanium diisopropoxide bis(acetylacetonate) (75%) in 1-butanol solution at 4000 rpm for 30 s, which was heated at 70^{o}C for 5 min. After the samples were cooled down to room temperature, the same process was repeated twice with 0.3 M titanium diisopropoxide bis(acetylacetonate) solution in 1-butanol. The coated FTO glass was annealed at 600 °C for 30min to obtain the compact TiO_2 electron selective layer and moved into N_2-purged glove box for device fabrication. These TiO_2 substrates were pre-heated to 90°C followed by the deposition of the perovskite photo-active thin films by spin-coating at 2000 rpm for 40s. The films were thermally annealed by a two-step annealing process at 110 °C for 60 mins, followed by 115 °C for another 30 mins. After cooled down to room temperature,

the hole transporting material Spiro-OMeTAD was spin-coated at 4000 rpm for 20 s, followed by the deposition of the top electrode of 90 nm patterned Au using thermal evaporation.

4. Perovskite solar cell measurement condition

After fabrication of perovskite solar cells, the device performance were measured in air at room temperature using an A.M. 1.5 solar simulator. Voltage was swept from 2V to -0.5V with a scan rate of 100 mV/s without any pre-condition before characterization.

5. Optical absorption spectrum of perovskite thin films and PbS nanoparticles

The optical absorption spectra of the thin films deposited with and without the addition of MAI-capped PbS nanoparticles were very similar to each other as shown in Figure S1(a), indicating the light harvesting of the small amount of PbS nanoparticles are trivial to the enhanced performance.

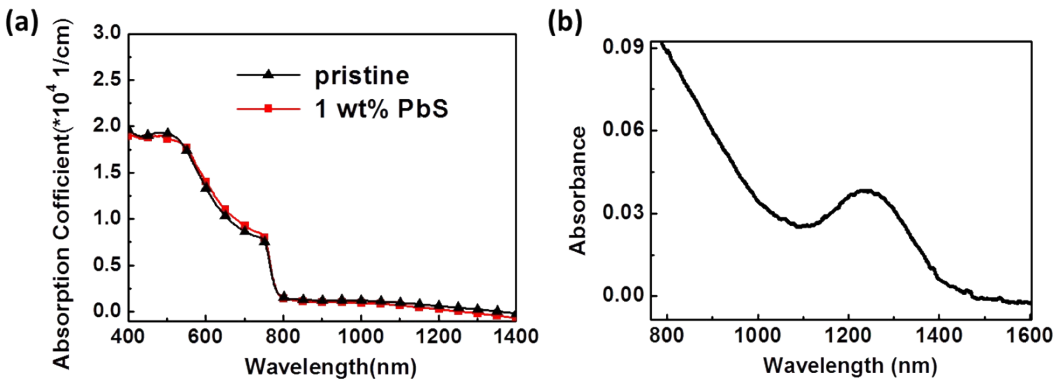

Figure S1. Optical absorption spectra of (a) perovskite thin films without and with 1 wt% PbS nanoparticles, and (b) the absorption spectrum for the equivalent PbS nanoparticles.

6. Gaussian fitting and Rietveld refinement of XRD spectra of perovskite thin films obtained from the θ-2θ scan data.

Figure S2 shows the Gaussian fitting of the (110) peaks obtained from the XRD θ-2θ scan data of perovskite thin films with and without incorporation of MAI-capped PbS nanoparticles. The resulting FMHW of each spectrum was summarized in Table S1, which shows increasingly sharpened peak widths with the increasing amount of PbS nanoparticles in the films; indicating the increasingly larger crystal sizes in the corresponding perovskite thin films.

For quantitatively analysis, we have conducted Rietveld refinement of the XRD spectra for the pristine perovskite films without and with 1.0 wt% MAI-PbS nanoparticles (obtained with θ-2θ scan). The results are presented in Figure S3 and Table S2. From the refinement fittings, the tetragonal lattice parameters together with a more biased (110) orientation factor $R_o = 0.551$ for the oriented perovskite crystals directed by MAI-PbS nanoparticles, compared to $R_o = 0.665$ for pristine film; for random orientation $R_o = 1$.[1,2] Moreover, scrutinizing the (110)

and (220) reflections of the XRD data, we found that the greatly enhanced (110)/(220) reflections of the perovskite crystals are accompanied by suppression of the neighboring (002)/(004) reflections, where these two crystal facets are perpendicular to each other. Based on these evidences, we suggest that the MAI-capped PbS nanoparticles may direct the perovskite crystal to preferentially grow along the film surface normal, with the (110) crystal plane.

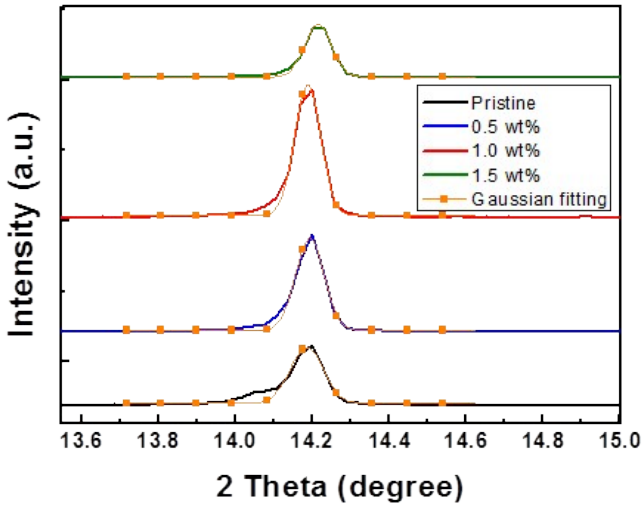

Figure S2. Gaussian fitting of (110) peaks from XRD θ-2θ scan data. Fitting results were shown in Table S1.

Table S1. FMHW of (110) peaks

Sample	Pristine	0.5 wt%	1.0 wt%	1.5 wt%
(110) peak width (FMHW)	0.0895°	0.0752°	0.0686°	0.0702°

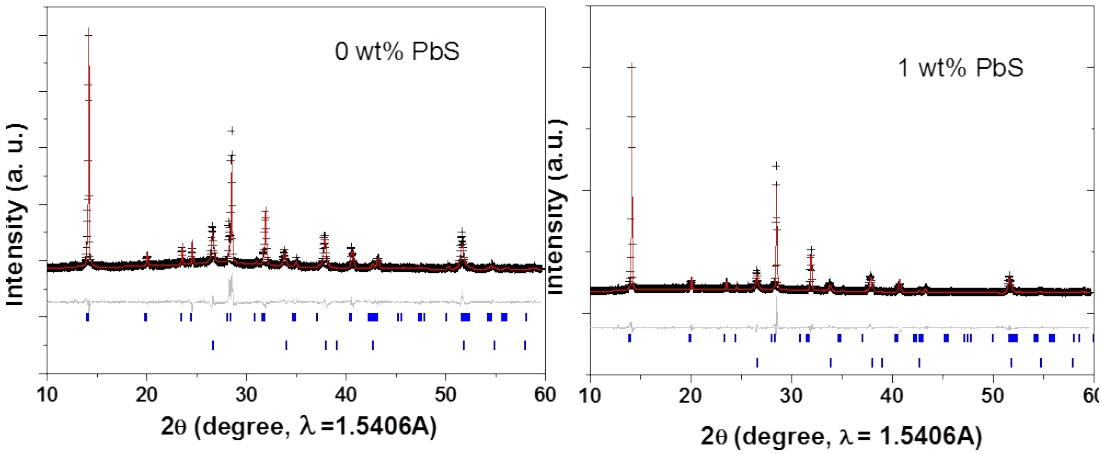

Figure S3. Reitveld refinement results for the XRD data measured for the $MAPbI_{3-x}Cl_x$ perovskite crystal thin films, without or with MAI-capped PbS nanoparticles.

Table S2. Tetragonal lattices (*a*=*b*,*c*) of the $MAPbI_{3-x}Cl_x$ perovskite crystal thin films, without or with the inclusion of PbS NPs, obtained using Reitveld refinement procedure of the XRD data.

	Film without PbS NPs	Film with 1 wt% PbS

		NPs
FTO preferred orientation factor in (101)	2.62(2)	2.69(3)
$MAPbI_{3-x}Cl_x$ preferred orientation factor R_o in (110)*	0.689(4)	0.551(4)
F_{osq} (002)	3.237E+05	1.089E+05
F_{osq} (110)	8.062E+05	7.121E+05
I(002)/I(110)	0.201	0.076
Lattice parameter		
$MAPbI_{3-x}Cl_x$ a (Å)	8.9138(2)	8.9058(1)
c (Å)	12.716(1)	12.680(2)
Vol.(Å^3)	1010.4(1)	1005.7(1)
wt%	60.6(2)	53.6(4)
FTO substrate a (Å)	4.7784(4)	4.7781(5)
c (Å)	3.2134(7)	3.213(1)
Vol.(Å^3)	73.37(1)	73.36(2)
wt%	39.3(3)	46.4(7)
Fitting accuracy		
wR_p	2.45%	3.30%
R_p	1.39%	1.72%
χ^2	1.368	1.383

F_{osq}: square of the observed structure factor, R_p: residual of least-square refinement, wR_p: weight residual, χ^2: goodness of fitting; *R_o = 1 for random orientation.

7. Device performance and film morphology with excess MAI content.

A controlled device prepared using the same amount of excess pristine MAI molecules (no PbS nanoparticles) identical to that of the 1.0 wt% device was also

fabricated for comparison. The resulted morphology and device performance are very similar to those of the pristine perovskite solar cell as shown in Figure S4, excluding the contribution of excess MAI molecules on the improved morphology and power conversion efficiencies.

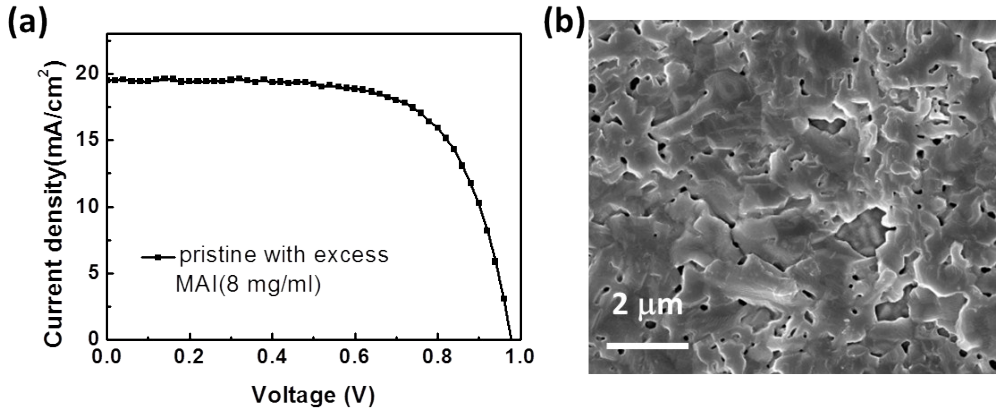

Figure S4. (a) device performance and (b) surface morphology of perovskite thin film fabricated with the same amount of excess pristine MAI molecules (no PbS nanoparticles) identical to the optimal 1.0 wt% device.

Table S3. Corresponding photovoltaic performance of Fig. S4(a).

V_{oc} (V)	J_{sc} (mA/cm^2)	FF (%)	PCE (%)
0.97	19.4	67.8	12.9

8. GIWAXS measurements

GIWAXS measurements were performed using the BL23A beamline station of the National Synchrotron Radiation Research Center (NSRRC) in Taiwan,[3] using a

flat-panel C10158DK-3957 area detector of a pixel size of 50 μm. With the sample surface defined in the x-y plane and the incident x-rays in the x-z plane, the wavevector transfer $\boldsymbol{q}$ = (q_x, q_y, q_z) of X-rays can be decomposed into three orthogonal components as follows: $q_x = 2\pi\lambda^{-1}(\cos\beta\cos\phi - \cos\alpha)$, $q_y = 2\pi\lambda^{-1}(\cos\beta\sin\phi)$, and $q_z = 2\pi\lambda^{-1}(\sin\alpha + \sin\beta)$ whereas α and β stand for incident and exit angles and ϕ measures the scattering angle away from the y-z plane.[4] Data were collected with a X-ray beam (λ =1.033 Å) of 0.2 mm diameter and a sample film incident angle of 2°; the sample-to-detector distances was 192 mm.

9. Transformed pole figure form 2D GIWAXS

There is missing wedge angle ±3.4° in the vicinity of the vertical direction of the pole figures transformed from the corresponding 2D GIWAXS patterns.

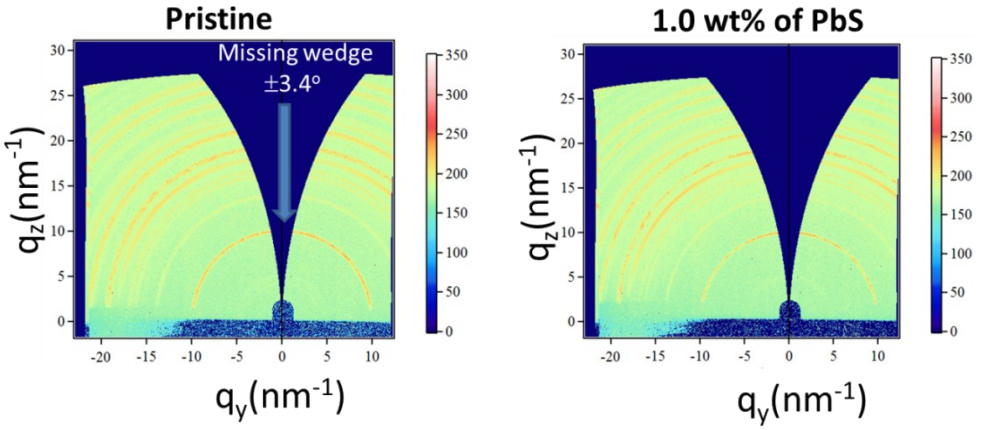

Figure S5. Pole figures transformed from the GIWAXS 2D patterns measured for

the $MAPbI_{3-x}Cl_x$ perovskite crystal thin films, without (pristine) or with MAI-capped PbS nanoparticles. The missing wedge angle in the azimuthal direction at $q \sim 10$ nm^{-1} , i.e. at the (110) reflection, is ±3.4° as indicated.

10. Diffusion model

The charge carrier diffusion lengths (L_D) of photo-generated carriers (electron and hole) can be estimated using a simple diffusion limited quenching model in a bilayer system. The photo-generated charge carrier density in the active layer can be described by a one-dimensional diffusion equation (eq. S1)[6-12]

$$\frac{L_D{}^2\partial^2(\delta n(x,t))}{\tau \quad \partial x^2} - \frac{\delta n(x,t)}{\tau} = \frac{\partial(\delta n(x,t))}{\partial t}$$

, where L_D is carrier diffusion length, τ is photo-generated carrier lifetime without quenching layer and $\delta n(x,t)$ is the photo-generated carrier concentration. x is the distance of a point in the active layer from the active layer/substrate interface.

By solving eq. S1 with two boundary conditions at t = 0,

$$\delta n(x,0) = \delta n(0,0) exp(\frac{-x}{\alpha})$$

, and when t is not zero,

$$\delta n(L,t) = 0$$

, time dependent carrier concentration N(t) which models the photo-generated

carrier decay behavior within active layer contacted with quenching layer can be obtained as the following eq. S2,

$$N(t) = \int_0^L \delta n(x,t)dx$$

$$= \frac{2\delta n(0,0)L}{\pi} exp(-\frac{t}{\tau}) \sum_{m=0}^{\infty} \left(exp(-\frac{\pi^2 L_D^2}{\tau L^2}(m+\frac{1}{2})^2 t) \frac{(-1)^m \exp(-\alpha L)\pi\left(m+\frac{1}{2}\right)+\alpha L}{(\alpha L^2+\pi^2\left(m+\frac{1}{2}\right)^2)(m+\frac{1}{2})} \right)$$

, where L is the thickness of active layer and α is absorption coefficient of active layer at the excitation wavelength.

In this work, perovskite films with L = 450 nm was excited by a pulse laser with wavelength at 466 nm. Absorption coefficient at 466 nm with $\alpha = 4.4 \times 10^4 cm^{-1}$ was accordingly applied for model fitting to obtain the carrier diffusion length L_D as presented in the manuscript.

Reference

1. W. A. Dollase, J. Appl. Cryst., 1986. **19**, 267-272.
2. A. March, Z. Kristallogr., 1932, **81**, 285-297
3. U.-S. Jeng, C. H. Su, C.-J. Su, K.-F. Liao, W.-T. Chuang, Y.-H. Lai, J.-W. Chang, Y.-J. Chen, Y.-S. Huang and M.-T. Lee, *Journal of Applied Crystallography*, 2009, **43**, 110-121.
4. (a) W.-R. Wu, U.-S. Jeng, C.-J. Su, K.-H. Wei, M.-S. Su, M.-Y. Chiu, C.-Y. Chen, W.-B. Su, C.-H. Su and A.-C. Su, *Acs Nano*, 2011, **5**, 6233-6243. (b) C.-M. Liu, Y.-W. Su, J.-M. Jiang, H.-C. Chen, S.-W. Lin, C.-J. Su, U.-S. Jeng and K.-H. Wei, *Journal of Materials Chemistry A*, 2014, **2**, 20760-20769.
5. (a) J. L. Baker, L. H. Jimison, S. Mannsfeld, S. Volkman, S. Yin, V. Subramanian, A. Salleo, A. P. Alivisatos, & M. F. Toney, *Langmuir* 2010,

26, 9146−9151. (b) J. Rivnay, S. C. B. Mannsfeld, C. E. Miller, A. Salleo, & M. F. Toney, Chem. Rev. 2012, **112**, 5488−5519.

6. J. E. Kroeze, T. J. Savenije, M. J. Vermeulen and J. M. Warman, *The Journal of Physical Chemistry B*, 2003, **107**, 7696-7705.
7. D. Zhitomirsky, O. Voznyy, S. Hoogland and E. H. Sargent, *ACS nano*, 2013, **7**, 5282-5290.
8. H. Najafov, B. Lee, Q. Zhou, L. Feldman and V. Podzorov, *Nature materials*, 2010, **9**, 938-943.
9. R. R. Lunt, J. B. Benziger and S. R. Forrest, *Advanced Materials*, 2010, **22**, 1233-1236.
10. A. Haugeneder, M. Neges, C. Kallinger, W. Spirkl, U. Lemmer, J. Feldmann, U. Scherf, E. Harth, A. Gügel and K. Müllen, *Phys Rev B*, 1999, **59**, 15346.
11. G. Xing, N. Mathews, S. Sun, S. S. Lim, Y. M. Lam, M. Gratzel, S. Mhaisalkar and T. C. Sum, *Science*, 2013, **342**, 344-347.
12. S. D. Stranks, G. E. Eperon, G. Grancini, C. Menelaou, M. J. Alcocer, T. Leijtens, L. M. Herz, A. Petrozza and H. J. Snaith, *Science*, 2013, **342**, 341-344.